Molecular Dynamics Simulations of Alkanes in the Zeolite Silicalite: Evidence for Resonant Diffusion Effects

Ron C. Runnebaum[†,‡] **and Edward J. Maginn***[,†]

Department of Chemical Engineering, and Center For Catalysis and Reaction Engineering, University of Notre Dame, Notre Dame, Indiana 46556

Received: March 3, 1997; In Final Form: May 7, 1997[⊗]

Molecular dynamics simulations have been conducted to study *n*-alkane dynamics in the zeolite silicalite. Chains ranging in length from *n*-C_4 to *n*-C_{20} have been examined at various loadings and temperatures. An interesting chain-length dependence for the individual components of the self-diffusivity tensor was observed. While the self-diffusivity of chains in the [100] and [001] directions exhibits a monotonic decrease as a function of chain length, the self-diffusivity along the [010] axis is a periodic function of chain length. Local maxima in the self-diffusivity along this axis occur for *n*-C_8 and *n*-C_{16}, while local minima are observed for *n*-C_6 and *n*-C_{14}. The apparent activation energy for diffusion is also periodic with chain length. Periodicity in the diffusivity and activation energies are most pronounced at low temperature. A physical explanation for this behavior is given in terms of a resonant diffusion mechanism. The essential features of previous theoretical treatments describing how resonant diffusion effects might occur in zeolites are confirmed by these simulations. Sorbate conformational structure and time constants for motion between channel systems are also computed. These calculations indicate that, at low temperature, long chains become localized in one channel system. Interchange between channels for these chains is very slow. Under these conditions, silicalite essentially acts as a one-dimensional zeolite. The fact that the time constant associated with molecular rearrangement may be greater than the time constant for diffusion along a given channel suggests a possible explanation for some of the differences often seen between zeolite self-diffusivities measured using transient and equilibrium techniques.

1. Introduction and Motivation

The dynamical behavior of molecules in zeolites and other molecular sieves has received widespread attention in recent years. Zeolites are used extensively as industrial catalysts[1] and are seeing increased use in separations applications, such as pressure swing adsorption (PSA)[2] and membrane-based separations.[3] In all cases, the dynamical behavior of sorbed molecules is critical in determining the performance of the catalytic or separation process. Predicting (or sometimes even understanding) the dynamics of sorbed molecules in molecular sieves is difficult. This is because the void spaces of molecular sieves have dimensions that are commensurate with the diffusing guest species, so that molecular-level guest−host interactions are the dominate factor in determining dynamical properties. Because it is difficult to assess the effect these interactions will have on the sorbate, diffusion in this "configurational" regime[4] is poorly understood.

Most of what is known about the dynamics of sorbates in molecular sieves comes from experimental work. Techniques for measuring sorbate diffusivities can be roughly divided into "macroscopic" and "microscopic" methods.[5] Macroscopic methods typically relate the dynamic response of a small zeolite sample to a perturbation in flow rate or concentration of the sorbate. Examples include the zero-length column (ZLC) technique,[6] frequency response methods,[7] and Wicke−Kallenbach (WK) membrane methods.[8] Microscopic techniques, on the other hand, enable the mean square displacement of the molecules sorbed inside the pores of a microporous material to be deduced under equilibrium conditions. Examples include pulsed-field gradient nuclear magnetic resonance (PFG NMR)[12] and quasi-elastic neutron scattering (QENS).[13] The self-diffusivity obtained from microscopic methods and the Fickian diffusivity obtained from macroscopic techniques can be compared through application of the so-called "Darken correction".[5] For many systems, the agreement between the diffusivities measured in these different experiments is quite good. However, there are a number of cases where the diffusivities predicted by these different methods disagree by one or more orders of magnitude. The source of this discrepancy has been the subject of much debate and is still not satisfactorily resolved.[5] As will be discussed in the Results section, the present study may help explain at least part of the discrepancy between these two measured quantities.

Very recently, molecular simulations have emerged as yet another technique that can be used to probe the dynamics of sorbates in molecular sieves. Details of the various molecular simulation techniques can be found in standard references.[14,15] An extensive review of past molecular modeling works involving molecular sieves can be found elsewhere.[16] Briefly, to model the dynamics of a sorbate inside the pores of a molecular sieve, an atomistic model is constructed of both the sorbate and microporous material. This model must faithfully capture the geometry and, importantly, the inter- and intramolecular energetic interactions that exist for the system. Equilibrium properties can be computed using Monte Carlo (MC) methods,[17] while equilibrium and dynamic behavior can be computed with a molecular dynamics (MD) technique.[18] In the present work, MD was used to compute the dynamical behavior of a series of

* Author to whom correspondence should be addressed. Email: maginn.1@nd.edu.

† Department of Chemical Engineering.

‡ Present address: Procter and Gamble Co., Winton Hill Technical Center, 6100 Hill Ave., Cincinnati, OH 45224.

§ Center for Catalysis and Reaction Engineering.

⊗ Abstract published in *Advance ACS Abstracts,* July 15, 1997.

S1089-5647(97)00774-8 CCC: $14.00

alkanes in the zeolite silicalite. Additional details of the MD method will be given in the next section.

Most of the simulation studies involving molecular sieves have focused on small, roughly spherical sorbates such as methane or the noble gases.[16] Computed equilibrium properties such as sorption isotherms and isosteric heats have agreed well with experimental measurements. Additional details that are hard to obtain experimentally, such as the preferred locations and conformations of sorbates, can also be obtained from simulations. Dynamic properties such as self-diffusivities have been computed with some success; self-diffusivities predicted by MD simulations typically agree well with values obtained from microscopic measurements but often do not agree as well with diffusivities obtained from macroscopic methods.

These early simulation studies have resulted in a much better understanding of the equilibrium and dynamic behavior of small sorbates in molecular sieves. However, only a limited number of applications involve the small molecules utilized in these early studies. To help understand the behavior of sorbates in zeolitic processes such as catalytic cracking and the separation of hydrocarbon isomers, molecular simulations must be carried out on larger, more complex species. Such simulations present a number of computational and methodological difficulties, which explains why there have been relatively few studies involving nonspherical sorbates. This has begun to change, however. Bandyopadhyay and Yashonath[19] have recently performed MC simulations of *n*-butane in zeolite Y, in which important conformational information was obtained. Klein et al.[20] and Demontis et al.[21] have conducted simulations of aromatic hydrocarbons in the zeolite NaY. These studies focused on the structure and energetics of the sorbed species. Insight into the mobility of the aromatics inside the zeolite pores was also obtained, although computational limits prevented diffusivities from being reliably estimated. Schrimpf and co-workers[22] have conducted MD simulations to compute the diffusivity of *p*-xylene in Na-Y. These workers carried out very long simulations with up to 24 total molecules. Despite the long simulation times, diffusivities could only be computed at high temperatures (greater than 500 K) due to the sluggishness of the bulky molecules. To overcome the computational limits of MD in tracking the motion of bulky molecules such as aromatics, Snurr et al.[23] used transition-state theory to estimate the diffusivity of benzene in silicalite. Due to its industrial significance, silicalite, the siliceous form of ZSM-5, has received a great deal of attention. June et al.[24] conducted MD simulations of *n*-butane and *n*-hexane in silicalite. Goodbody and co-workers[25] used MD to simulate methane and *n*-butane in silicalite. Catlow and co-workers[26−28] have also used MD to simulate hydrocarbons as long as *n*-hexane in silicalite. These studies all indicate that self-diffusivities in silicalite for molecules in the C_3 to *n*-C_6 range are on the order of 1×10^{-9} m^2/s, in good agreement with PFG NMR and QENS measurements. The simulations also indicate that the zeolite dominates the conformational structure as well as the dynamics of the sorbates. That is, sorbate−sorbate interactions play a secondary effect in determining the dynamic behavior of the sorbates.

Few simulation studies have been conducted that investigate the behavior of chains longer than *n*-hexane in zeolites. Smit and co-workers[29−34] performed MC simulations to compute the equilibrium properties of chains as long as *n*-decane in silicalite. Maginn et al.[35,36] computed equilibrium properties of chains as long as *n*-C_{20} at infinite dilution using an MC integration technique. These studies suggest that, due to registry effects between the chain and zeolite channels, equilibrium properties such as isosteric heats and adsorption isotherms can show anomalous behavior as a function of chain length. This observation is consistent with recent experimental findings. For example, Smit and Maesen[32] computed sorption isotherms for a series of linear alkanes in silicalite. Their results show a "step" in the isotherm for *n*-C_8. They attributed the step to a "commensurate freezing" mechanism in which chains of a particular length become localized in certain regions of the zeolite. Recent experimental isotherm measurements by Sun et al.[37] show the same qualitative features as the MC simulations.

While the studies mentioned above have begun to shed light on the *equilibrium* behavior of long chains in silicalite, the *dynamics* of long chains has not been widely investigated with molecular simulations. This is mainly due to computational limits. ZLC measurements by Eic and Ruthven[38] have determined that the self-diffusivity of *n*-C_{10} in silicalite is on the order of 1×10^{-13} m^2/s, which is too small to be tracked with conventional MD.[39] As was mentioned earlier, however, there are often discrepancies between macroscopic experiments (such as the ZLC method) and microscopic methods (such as PFG NMR). For example, the same set of ZLC measurements in ref 38 yielded a self-diffusivity for propane in silicalite of 7.7×10^{-12} m^2/s, while PFG NMR measurements by Caro and co-workers[40] gave a value of 3.9×10^{-9} m^2/s. Diffusivities of the latter value are accessible to MD simulations. To investigate the dynamics of long chains and circumvent possible time scale problems, Maginn et al.[41] recently carried out a simulation study in which the self-diffusivities of chains ranging in length from *n*-C_4 to *n*-C_{20} were computed using a hierarchical, coarse-grained simulation technique. This method utilizes Brownian motion and transition-state theories and is capable of probing phenomena on the microsecond time scale using modest computational resources. The self-diffusivities computed with this technique agreed well with microscopic measurements for short chains but predicted self-diffusivities that were much higher than the ZLC experiments for chains in the C_{10}−C_{20} range. To our knowledge, *n*-C_6 is the longest chain in silicalite that has been examined using NMR,[42] so a direct comparison with microscopic measurements is not possible. The relatively high values of the diffusivity predicted in the coarse-grained simulation study, however, suggest that MD may be capable of estimating diffusivities for fairly long chains in silicalite. This was a major motivating factor for initiating the present work. In addition to predicting self-diffusivities, MD simulations can provide information on the mechanism of chain diffusion in silicalite. These details were not captured by the coarse-grained model and are difficult to obtain experimentally.

Another motivating factor for studying the diffusion of chain molecules in zeolites is to investigate the so-called "window effect". The window effect was first reported by Gorring in 1973.[43] In this work, macroscopic diffusivity measurements were made for a series of normal alkanes in zeolite T. Instead of declining steadily as a function of chain length, as is seen in a homogeneous phase, Gorring found that the diffusivities exhibited local maxima and minima at chain lengths that correlated with the periodicity of the zeolite lattice. Theoretical explanations for this behavior in terms of a "resonant diffusion" mechanism were subsequently put forth.[44−46] These theoretical treatments, which will be discussed in more detail later, helped provide a reasonable explanation for Gorring's findings. There is some debate, however, as to the physical origin of the window effect. It has been suggested[5] that the experimental procedure used by Gorring is subject to extraneous heat and mass transfer effects, which might be responsible for the periodicity in the diffusivity as a function of chain length. To our knowledge, there have been no other published experimental reports of a

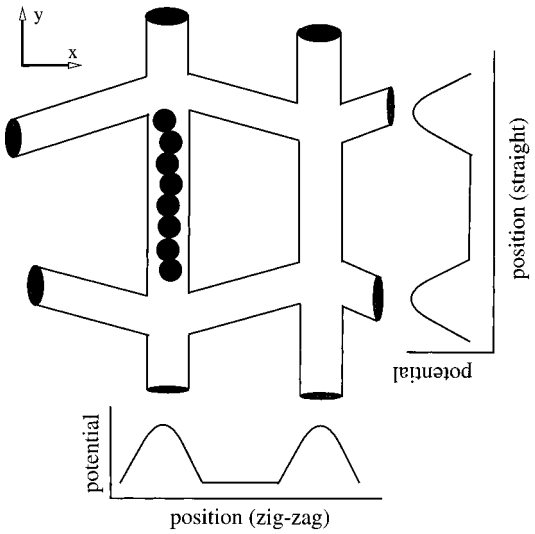

Figure 1. Schematic of the structure of the silicalite lattice. "Straight" channels allow movement in the [010] or "*Y*"-direction, while sinusoidal or "zigzag" channels allow motion in the [100] or "*X*"-direction. The intersection of these two channels represents a potential energy barrier. The distance between adjacent barriers is roughly equal to the length of an extended *n*-octane molecule.

window effect in zeolites nor have Gorring's results been reproduced. Molecular simulations are ideally suited to test these theories to see under what circumstances, if any, resonant diffusion effects in zeolites can be expected.

Before moving on, it should be noted that other theories have predicted anomalous diffusion behavior when sorbates "fit" a certain way inside zeolite pores. For example, Derouane et al.[47] proposed a theory that predicts anomalous diffusion behavior when the curvature of a zeolite pore matches a certain characteristic length scale of the sorbate. Basic elements of this theory have been confirmed by the MD simulations of Yashonath and Santikary,[48] in which the dependence of the self-diffusivity for Lennard-Jones spheres was found to depend strongly on the ratio of the pore to molecular diameter.

Below we report the results of an MD study of normal alkane sorbates in the zeolite silicalite. Silicalite was chosen for this work because of the industrial importance of the isostructural ZSM-5 and because the diffusion of small molecules in silicalite has been extensively studied experimentally and computationally. While silicalite does not have the cage-and-window structure of zeolite T,[49] sorbed alkanes do experience a periodically varying potential energy field within the pores of silicalite, and so it can serve as a test of the resonant diffusion theories. Other zeolitic structures can easily be examined with MD. Chains ranging in length from *n*-C_4 to *n*-C_{20} were examined at temperatures of 300, 350, and 400 K. To our knowledge, this is the first molecular simulation study that has examined the detailed dynamics of chain molecules longer than *n*-hexane in zeolites. It is also the first simulation study in which the ratio of chain length to lattice periodicity was varied systematically to gauge the effect this ratio has on chain dynamics. In the following sections, details of the model and simulation methodology will be given, followed by a presentation and discussion of the results of the simulations and a brief summary.

2. Model

Silicalite is the aluminum-free form of the zeolite ZSM-5. The channel system consists of two sets of interconnected pores, each having a diameter of roughly 5.5 Å. Figure 1 depicts a schematic of the channel system. Motion in the [100] direction takes place along serpentine "zigzag" channels, while in the [010] direction the channels are essentially "straight". These two channels meet at a relatively open "intersection" region, having a roughly spherical shape with diameter of about 8 Å. In the following, we will use the terms zigzag, straight, and intersection in referring to these regions within the silicalite lattice. Motion in the [001] direction is possible only by moving along a tortuous path between straight and zigzag channels via the intersection regions. Previous simulation work[24] has shown that the lowest energy state for a hydrocarbon in silicalite is in the straight and zigzag channels, where favorable dispersion interactions with the pore walls are greatest. The channel intersection regions represent high-energy barriers, as depicted schematically in Figure 1. This is because a chain in the open intersection regions loses intimate contact with the lattice atoms, thus giving up favorable dispersion interactions. Note that silicalite is opposite of some zeolites, where constrictions or "windows" represent high-energy regions.

For this work, the orthorhombic form of silicalite having *Pnma* symmetry was used.[50] Atomic positions were taken from X-ray diffraction data.[51] In line with previous studies,[36] the lattice was taken as rigid to reduce computational requirements. This assumption has been shown to be acceptable for sorbates that do not fit tightly in the pores of the zeolite.[52,53] The model for the alkanes is the same as that used in previous work.[41] The appropriate number of united atom interaction sites were connected by infinitely stiff harmonic bonds.[54] Bond angles and torsion angles were allowed to fluctuate under the influence of an appropriate potential.[55] Intramolecular interactions were taken into account for chains longer than *n*-butane through use of a 12-6 Lennard-Jones potential. Zeolite−alkane interactions were also represented with a 12-6 potential. Each alkane interaction site was assigned the same set of Lennard-Jones interaction parameters. The "methyl" and "methylene" groups of the chains were assigned masses of 15 and 14 amu, respectively. Because we were most interested in the way the zeolite potential field affects chain mobility, most of the simulations were performed in the infinite dilution limit (i.e. intermolecular interactions were turned off). A small number of simulations were performed at finite loadings to gauge the effect this has on static and dynamics properties. A 13 Å cutoff radius was employed in computing the Lennard-Jones interactions. For the simulations performed at finite loading, a neighbor list was used with a skin thickness of 1.08 times the cutoff radius. The form of the force field, along with a complete listing of parameters, can be found elsewhere.[36] While several other force fields have been used in simulations of alkanes,[56] the force field used in the present study has been shown to adequately reproduce experimental sorption thermodynamic data for chains as long as *n*-C_{10} in silicalite. It is also capable of closely matching the experimentally measured dynamics of small molecules such as *n*-butane and *n*-hexane in silicalite.[24,26] It is therefore reasonable to extend the model to longer chains. More detailed force fields are also being examined in our laboratory.[57]

3. Molecular Dynamics Technique

The simulations were conducted by integrating the classical equations of motion using a fifth-order predictor−corrector algorithm with a 2 fs time step.[58] Simulations were performed at 300, 350, and 400 K to assess the effect temperature has on the static and dynamic properties. To emulate the energy exchange processes that would occur using an animated lattice, a thermostating technique was used to maintain the temperature near the set point.[59] The "time constant" for thermal energy

exchange was set at 1 ps, which roughly corresponds to the time it takes for a small molecule to "rattle" within the pores of silicalite. Other thermostating techniques[14] were tested and found to yield essentially the same results.

To begin a simulation, a predetermined number of chains were placed inside the zeolite. Low-energy starting configurations were generated by using a configurational-bias Monte Carlo method to "grow" the chains inside the pores.[36] After these low-energy configurations were generated, the system was equilibrated by carrying out MD for 2 ns. To ensure that the system had indeed relaxed to a state representative of an equilibrium configuration, static properties such as dihedral angle distributions and siting probabilities were computed and found to agree with values calculated in previous MC simulations.[36] After the equilibration period, MD simulations were conducted for an additional 10 ns, during which conformational information was recorded to disk. Note that these simulations are much longer than what has been used in previous studies[60] and required the use of a highly optimized MD code.[61] Long simulations are needed to track the relatively slow motion of the longer chains. As will be discussed below, some dynamical processes take place over time scales that are still orders of magnitude longer than these simulations. Nevertheless, it will be shown that most of the salient dynamics can be adequately captured over the course of a 10 ns simulation. By invoking assumptions regarding the nature of long-time relaxation processes, reasonable estimates for the time constants of these processes can be extrapolated from the short-time simulations.

In most cases, 128 molecules were used in the simulations. For the longest chains at infinite dilution, simulations were carried out using as few as 32 molecules to reduce the computational requirements. To test the impact of this on computed properties, infinite dilution simulations were conducted for *n*-C_{20} at 300 K using 32 and 128 molecules. There was no discernible difference in the static or dynamic results of these simulations. This is consistent with the expectation that system size effects are smallest in the case of infinite dilution simulations. The use of fewer than 32 molecules might not enable all regions of the zeolite to be adequately probed by sorbates, so this was taken as the minimum number of chains. At finite loadings, at least 64 molecules were used in all cases.

4. Results

We begin by discussing the results of calculations performed in the limit of an infinitely dilute sorbate phase. Later, we discuss results at finite loadings.

4.1 Infinite Dilution. The self-diffusion coefficient, D_s, was computed for each simulation using the Einstein equation

$$D_s = {}^1/_6 \lim_{t\to\infty} \frac{d}{dt}\langle(\mathbf{r}(t) - \mathbf{r}(0))^2\rangle \qquad (1)$$

where the term in pointed brackets refers to an ensemble average of the mean square displacement (MSD) of a chain. Because silicalite is anisotropic, the diagonal terms of the self-diffusivity tensor were computed using the following equation

$$D_{s,\alpha\alpha} = {}^1/_2 \lim_{t\to\infty} \frac{d}{dt}\langle(r_\alpha(t) - r_\alpha(0))^2\rangle \qquad (2)$$

where α refers to either the *X*, *Y*, or *Z* Cartesian component of the position vector. A block averaging technique[14] was used to improve the statistics. Figure 2 shows a representative plot of the MSD versus time for *n*-octane at 350 K along the [100] (zigzag channels), [010] (straight channels), and [001] (tortuous path) directions. The slopes of these curves at long time are proportional to the appropriate component on the self-diffusivity tensor, $D_{s,\alpha\alpha}$. An important consideration in the use of eq 1 is that the simulations must be long enough to ensure that true diffusive motion is observed. That is, the MSD must be linear over the range at which the diffusivity is estimated. The results in Figure 2 show that, for *n*-octane at 350 K, this linear behavior is achieved well within the 2.5 ns correlation time shown in the figure. For each chain length and temperature examined, the linearity of the MSD versus time was confirmed before computing the self-diffusivity. Other criteria, such as how far the chains moved during a given simulation, were also monitored to ensure that true diffusive motion was being observed.[62]

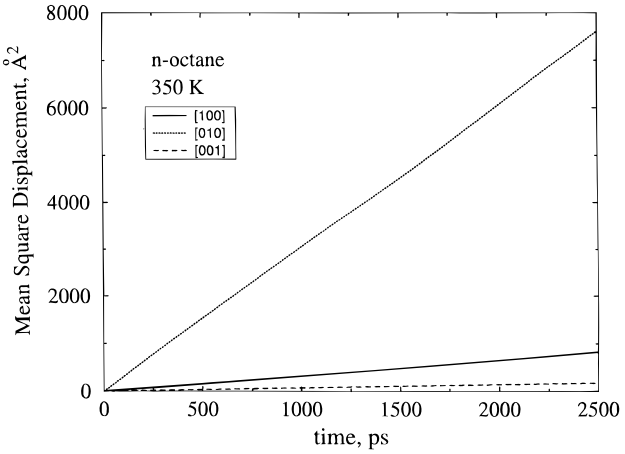

Figure 2. Mean square displacement as a function of time for *n*-octane at 350 K along the three principle axes of silicalite. Motion along the straight channels (the [010] direction) is much more facile than in other directions.

Before discussing the diffusivity results in detail, we note that the present MD work is expected to yield an *upper limit* on the actual self-diffusivity of the system. There are three primary reasons for this. First, the zeolite lattice is modeled as a siliceous perfect crystal. It is generally believed that lattice defects and acid sites associated with aluminum atoms inhibit the mobility of sorbates. Defects and aluminum atoms are inevitable in real zeolite samples, but these effects are not treated in our model. Second, most of the MD simulations were conducted in the infinite dilution limit. Previous work[24,42,63] has shown that the self-diffusivity in silicalite decreases as a function of loading. Because experimental studies are necessarily conducted at finite loading levels, it is reasonable to expect that experimental results will exhibit lower diffusivities than the simulations. Results from MD simulations at finite loadings (discussed below) support this conclusion. When possible, we have chosen to compare our infinite dilution results with experimental values at the lowest loading reported. Finally, we have used a united atom model for the alkanes. It has been shown that united atom models can yield enhanced local mobilities over what would be seen with explicit atom models.[64]

Figure 3 is a plot of D_s as a function of chain length at 300 K. The open circles are the results obtained in the present study. Also shown are previous MD simulation results[24] and "microscopic" experimental results obtained using the following techniques: pulsed field gradient NMR (PFG NMR)[42] and quasi-elastic neutron scattering (QENS).[65,66] We have plotted the results from only two macroscopic experimental studies: a ZLC study conducted by Eic and Ruthven[38] and a recent Wicke−Kallenbach (WK) embedded crystal study by Sun et al.[11] Note that the experimental results actually represent the "corrected diffusivity", which is equal to the self-diffusivity in

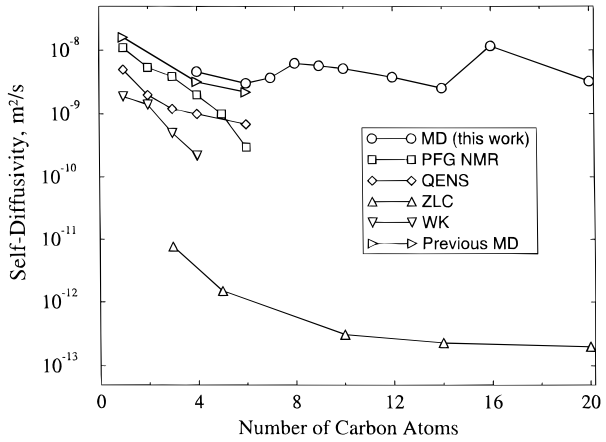

Figure 3. Self-diffusivities as a function of chain length near 300 K. See text for references to the various data sets.

the limit of low loadings.[5,63] A number of other macroscopic results for hydrocarbons in silicalite have been summarized in a recent paper[41] and are not reproduced here. The ZLC study was chosen because, to our knowledge, it is the only set of published experimental diffusivities for alkanes longer than *n*-C_6 in silicalite. The WK results are shown because they represent recent data that is thought to be free from extraneous effects that could skew the measured diffusivities.[11] We should point out that the large differences between the microscopic and macroscopic results are typical. The diffusivities for short chains reported in the ZLC study agree more or less with other macroscopic experiments.[41]

We begin by examining the predicted self-diffusivities for short chains (C_1-C_6). There is fairly good agreement between the MD results of this work and previous MD, NMR, and QENS studies. As expected the MD results form an upper bound on experimentally determined self-diffusivities. It will be shown later that experimental activation energies for diffusion are also captured well by the MD simulations. As is often the case, the MD and "microscopic" experimental results are much higher than the values typically determined by "macroscopic" methods,[5] as represented by the ZLC data. It is interesting to note that, while the macroscopic ZLC diffusivities are about 3 orders of magnitude lower than the values obtained in the MD, NMR, and QENS techniques, the agreement between the WK results and the microscopic methods is much better. Sun et al.[11] claim that their WK technique is more accurate than other macroscopic methods, since it is a direct technique in which extraneous heat and mass transfer effects are minimized. When viewed in light of the simulation results and other experimental methods, these data suggest that the actual self-diffusivity of short alkanes in silicalite is probably closer to 1×10^{-9} m^2/s than the value reported in previous macroscopic methods (1×10^{-12} m^2/s). Due to the difficulty of the experiments and the variability inherent in the use of different samples, it is doubtful that anything other than order of magnitude precision can be obtained in diffusivity measurements.

For chains longer than C_6, there is only the ZLC study to compare our results with. Given the level of disagreement between the MD and ZLC results for short chains, it is not surprising that this disagreement persists for the longer chains. Nevertheless, the *trends* exhibited by the two studies are intriguing. The ZLC measurements show the surprising result that the self-diffusivities decline slightly as a function of chain length for the shortest chains, and then actually level off for the longest chains. D_s is practically independent of chain length for alkanes longer than C_{10}. The MD results show a similar pattern, albeit at much higher values of D_s. A slight enhancement in D_s is seen at C_8 and C_{16}. A molecular-level interpretation for this behavior is given below. We note that an earlier theoretical study[41] predicted a similar trend in the self-diffusivity as a function of chain length. Additional experimental studies for longer alkanes should be carried out to help shed light on this behavior.

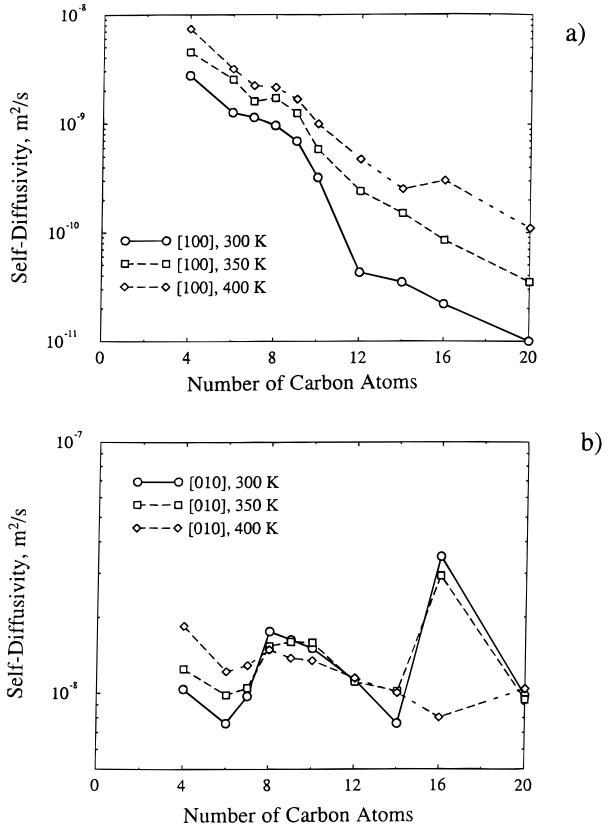

Figure 4. (a) Computed values of $D_{s,xx}$ shown as a function of chain length and temperature. $D_{s,xx}$ decreases steadily with increasing chain length and with decreasing temperature. (b) The same results shown for $D_{s,yy}$, which characterizes the mobility along the straight channels. Notice that the self-diffusivity along this direction is much higher than that along the *X*-direction. In addition, $D_{s,yy}$ is periodic with chain length, which indicates a resonant diffusion phenomena along this direction.

To interpret the results in Figure 3, it is instructive to look at the individual components of the self-diffusivity tensor. The anisotropy of D_s can be clearly seen from Figure 2. Translation along the straight channels is more facile than motion in the other two directions. Figure 4 shows the dependence of $D_{s,xx}$ and $D_{s,yy}$ on chain length and temperature. $D_{s,zz}$ exhibits the same basic trends as $D_{s,xx}$, and so is omitted for clarity. Table 1 provides a complete listing of all computed self-diffusivities. Examination of Figure 4 reveals a number of interesting features. First, while $D_{s,xx}$ steadily decreases as a function of chain length at fixed temperature, $D_{s,yy}$ is an oscillatory function of the number of carbon atoms in the chain. This trend is most apparent at low temperature, where local minima are seen in $D_{s,yy}$ near *n*-C_6 and *n*-C_{14} and local maxima appear for *n*-C_8 and *n*-C_{16}. The relative magnitudes of the maxima in $D_{s,yy}$ decrease as temperature increases. At 400 K, $D_{s,yy}$ is nearly constant as a function of chain length. Because D_s is the sum of the three individual components ($D_s = {}^1/_3[D_{s,xx} + D_{s,yy} + D_{s,zz}]$), it appears to be essentially independent of chain length in Figure 3. However, the behavior of $D_{s,yy}$ is suggestive of a "resonant diffusion" mechanism along the straight channels of silicalite.

The concept of resonant diffusion, which was touched on briefly in the Introduction, has been proposed as an explanation

TABLE 1: Computed Self-Diffusivities in Units of $\times 10^{-9}$ m^2/s[a]

N	q	T (K)	$D_{s,xx}$	$D_{s,yy}$	$D_{s,zz}$	D_s
4	0	300	2.74	10.4	0.70	4.61
6	0	300	1.26	7.59	0.28	3.04
7	0	300	1.14	9.73	0.27	3.71
8	0	300	0.96	17.6	0.20	6.23
9	0	300	0.69	16.3	0.10	5.71
10	0	300	0.32	15.1	0.062	5.17
12	0	300	0.043	11.3	0.008	3.79
14	0	300	0.035	7.69	0.008	2.58
16	0	300	0.022	39.6	0.003	13.2
20	0	300	0.010	9.77	0.001	3.13
6	0.5	300	1.20	6.1	0.30	2.50
7	0.5	300	0.86	7.7	0.25	2.95
8	0.5	300	0.68	12.0	0.19	4.20
9	0.5	300	0.52	10.6	0.075	3.70
10	0.5	300	0.28	8.0	0.068	2.80
16	0.5	300	0.030	21.5	0.0036	7.18
6	5.3	300	0.19	1.16	0.043	0.46
8	4.0	300	0.040	0.063	0.0045	0.036
12	2.7	300	0.032	0.18	0.0034	0.073
16	2.0	300	0.028	0.37	0.0018	0.13
4	0	350	4.49	12.5	1.34	6.12
6	0	350	2.52	9.84	0.51	4.29
7	0	350	1.59	10.5	0.46	4.17
8	0	350	1.70	15.4	0.34	5.80
9	0	350	1.24	16.0	0.23	5.83
10	0	350	0.58	15.9	0.15	5.54
12	0	350	0.24	11.1	0.061	3.82
14	0	350	0.15	10.23	0.030	3.47
16	0	350	0.085	29.3	0.016	9.80
20	0	350	0.035	9.42	0.004	3.15
4	0	400	7.35	18.5	1.49	9.11
6	0	400	3.13	12.2	0.83	5.40
7	0	400	2.21	12.9	0.63	5.26
8	0	400	2.13	14.9	0.42	5.83
9	0	400	1.66	13.8	0.39	5.27
10	0	400	0.99	13.5	0.32	4.94
12	0	400	0.47	11.5	0.18	4.03
14	0	400	0.25	10.1	0.073	3.46
16	0	400	0.30	8.03	0.035	2.79
20	0	400	0.11	10.39	0.029	3.51
6	0.5	400	2.55	8.35	0.68	3.90
7	0.5	400	1.85	6.90	0.74	3.15
8	0.5	400	1.50	9.20	0.57	3.80
9	0.5	400	1.10	12.0	0.041	4.60
10	0.5	400	1.10	9.10	0.022	3.40

[a] N is the number of carbon atoms in a chain, and q is the loading in molecules/unit cell.

for experimentally observed oscillations in diffusivities as a function of the length of sorbate chains in zeolite T (the so-called "window effect").[43] Ruckenstein and Lee[44] proposed a conceptual theory based on symmetry arguments, which showed that resonant diffusion could occur whenever the length of the diffusing molecule is an integral multiple of the periodicity of the host lattice. This model was subsequently expanded upon by Nitsche and Wei[45] and by Tsekov and Ruckenstein.[46] These models treat the sorbate molecules as rigid rods diffusing in a one-dimensional potential field consisting of periodic potential barriers. They predict that maxima in the diffusion coefficient occur whenever the ratio of the chain length to the length between potential energy barriers is an integer, while minima occur whenever the ratio is a half-integer. The models also predict that apparent activation energies for diffusion should approach zero as the ratio of chain length to external potential wavelength approaches an integer value. Conversely, the apparent activation energy should be a maximum when this ratio is a half-integer value.

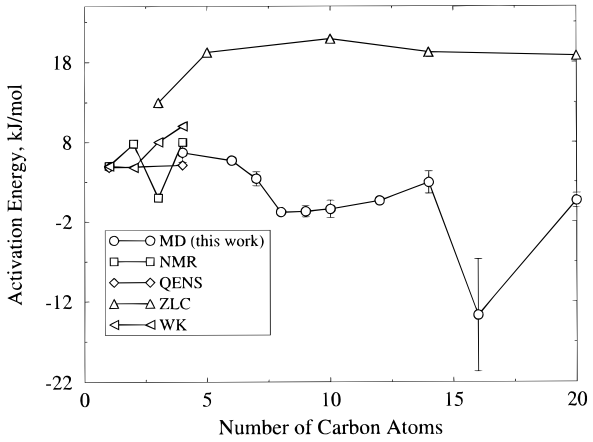

Figure 5. Apparent activation energy for diffusion in kJ/mol as a function of chain length. Experimental values are taken from the literature (see text for citations).

TABLE 2: Computed Apparent Activation Energy for Diffusion at Infinite Dilution in Units of kJ/mol

N	E_{act}	N	E_{act}
4	6.69 ± 1.2	10	-0.4 ± 1.1
6	5.7 ± 0.2	12	0.64 ± 0.4
7	3.4 ± 0.9	14	2.95 ± 1.4
8	-0.8 ± 0.4	16	-13.7 ± 7
9	-0.7 ± 0.7	20	0.67 ± 0.9

To examine the unusual dynamic behavior of the chains in greater detail, apparent activation energies for diffusion and chain end-to-end length distributions were computed for each species. We define the apparent activation energy for diffusion, E_{act}, by the following equation

$$D_s = D_0 \exp[-\beta E_{act}] \quad (3)$$

where D_0 is a preexponential factor and $\beta = 1/k_B T$, with k_B equal to the Boltzmann constant and T the temperature. Figure 5 shows the computed apparent activation energy for diffusion, along with experimental values taken from the literature. Table 2 provides a summary of all computed activation energies. As with the self-diffusivity in Figure 3, the MD predictions for short chains show fairly good agreement with the NMR, QENS, and WK results but predict a lower activation energy than the ZLC results. For longer chains, the MD results predict that the apparent activation energy for diffusion approaches zero and even becomes negative at certain chain lengths. Again, the minima in the activation energies correspond with the maxima in D_s, which is consistent with the predictions of the resonant diffusion models. An explanation for the negative apparent activation energies for diffusion, meaning that diffusivities *decrease* as temperature increases, will be given later.

Since the resonant diffusion mechanism is dependent on the ratio of chain length to lattice periodicity, we now examine the distribution of chain lengths in the zeolite. Figure 6 shows the distribution of end-to-end distances for *n*-C_8, *n*-C_{12}, and *n*-C_{16} chains located along the straight channels as a function of temperature. The sharp peaks at roughly 9, 14, and 19 Å correspond to chains stretched in nearly all-*trans* conformations. Note that the lattice periodicity of silicalite in the [010] direction is 9.96 Å. Therefore, the large peaks for C_8 and C_{16} correspond to chains that are very close to the "resonance length" of the lattice. On the other hand, the large peak for C_{12} is very near a half-integer value of the lattice periodicity. Notice also that the heights of the peaks corresponding to stretched conformations decrease as temperature is increased. The shoulder at smaller end-to-end distances corresponds to chains aligned along

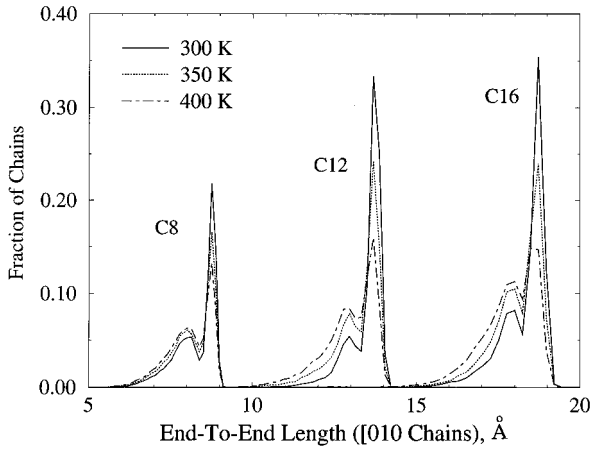

Figure 6. End-to-end length distribution for C_8, C_{12}, and C_{16} chains located along the straight channels as a function of temperature. The periodicity of silicalite along the [010] direction is 9.96 Å. The large peaks correspond to "stretched" chains existing in essentially all-*trans* conformations. The peaks for C_8 and C_{16} are nearly at the lattice resonance length, while the large peak for C_{12} is at a half-integer value of the lattice periodicity. Increasing the temperature reduces the number of chains at the resonance length.

the straight channels that have some degree of *gauche* or "kinked" character. The *gauche* peak grows as temperature increases. This is the direct consequence of higher entropy conformations being favored at high temperature. Note that the curves in Figure 6 are for chains aligned along the straight channels and are normalized by the total number of chains. More C_{16} chains align along the straight channels than do C_8 chains,[36] which explains why the areas under the C_{16} curves are greater than those under the C_8 curves.

To be more quantitative in probing whether the unusual behavior seen in the simulations was caused by a resonant diffusion mechanism and to understand the trends seen for all chain lengths, a resonance parameter, λ, can be defined as[45]

$$\lambda \equiv L/l \tag{4}$$

where L is the most probable end-to-end chain length for chains aligned along the straight channels and l is the zeolite lattice periodicity along the straight channels (corresponding to the distance between channel intersection centers). Values of $\lambda =$ 1.0, 2.0, ... indicate a good "fit" between the most probable chain length and the lattice. If the resonant diffusion model is operational, chains having λ near these integer values will show higher diffusivities and lower apparent activation energies than chains with half-integer values (i.e. $\lambda = 0.5, 1.5, ...$). Note, however, that λ only gives an *approximate* measure of the fit of the chains in the lattice and thus provides only a rough gauge as to when resonant diffusion effects should be expected. This is due to two factors. First, chains actually sample a distribution of lengths, while λ is based on the most probable length. This can clearly be seen by examining Figure 6. Alkanes experience a multidimensional potential energy hypersurface as they diffuse through the zeolite channels. The resonant diffusion models are based on rigid rods diffusing through a one-dimensional potential energy field. Second, while the lattice periodicity of silicalite in the [010] direction is $l = 9.96$ Å (as defined by the distance between channel intersection midpoints), the high-energy intersection regions have a finite volume. That is, the high-energy portion of the intersections extend $1-2$ Å on either side of the intersection midpoint long the straight channel. This energy barrier does not vary smoothly but is instead a complicated function of chain location and conformation.

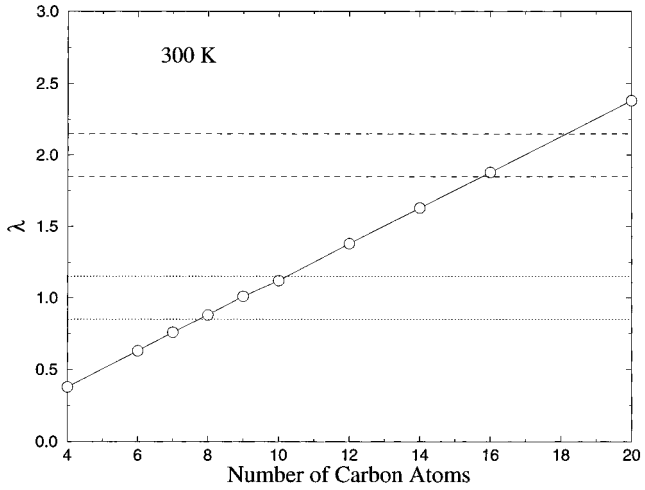

Figure 7. Resonance parameter, λ, as a function of chain length. Dotted and dashed lines encompass chain regions of λ where resonant diffusion effects are expected.

Keeping in mind the limitations of λ in predicting the onset of resonant diffusion behavior, we now examine the dependence of λ on chain length and compare this to computed self-diffusivities and activation energies. Figure 7 shows the values of λ for chains aligned along the straight channels of silicalite at 300 K. Notice that λ is essentially linear as a function of chain length. This is consistent with the finding that the zeolite channels force chains to adopt highly stretched conformations so that the length of a chain is nearly proportional to the number of atoms. The dotted lines mark the region where $\lambda = 1.0 \pm 0.15$, and the dashed lines show where $\lambda = 2.0 \pm 0.15$. On the basis of a knowledge of the size of the channel intersections, these "resonant diffusion zones" approximately encompass the regions where the influence of the high potential energy intersections is felt by the chains. If the resonant diffusion mechanism is operational, chains having a length which falls within these zones should exhibit stronger resonant diffusion characteristics than chains outside these regions. That is, C_8, C_9, and C_{10} are expected to have higher diffusivities and lower activation energies for diffusion than C_4, C_6, and C_7 as well as for C_{12} and C_{14}. The same trend should be seen for C_{16} relative to C_{12} and C_{14}, with diffusivity then dropping and activation energy rising for C_{20}. Examination of the data in Figures 4b and 5 as well as Tables 1 and 2 shows that the trends predicted by invoking the resonant diffusion model do in fact occur for all the chain lengths studied here. $D_{s,yy}$ rises and E_{act} falls as λ approaches 1.0 and 2.0. Chains having λ within the resonant diffusion zones of Figure 7 have higher self-diffusivities and lower activation energies for diffusion than those outside the resonant diffusion zones. This qualitative agreement between the resonant diffusion model (appropriately extended to account for flexible chains and the finite size of the zeolite potential energy barriers) and the simulation results suggests that a resonant diffusion mechanism is operational along the straight channels of silicalite. To test the model further, additional simulations should be performed. In particular, the analysis here and the data in Figure 7 suggest that the next resonance peak will occur for *n*-C_{23} and *n*-C_{24}. We would also expect that the diffusivity of *n*-C_{17} and *n*-C_{18} (which should fall within the second resonant diffusion zone) to be enhanced relative to *n*-C_{20}. Future simulations can test these predictions to see if the model still remains valid.

Other interesting trends can be seen upon closer inspection of the results. C_{12}, which falls outside a resonant diffusion zone, has a higher self-diffusivity and lower activation energy than C_6, which also falls outside a zone. The simple resonant

diffusion model cannot account for the differences between these two chains. Clearly, the multidimensional nature of the potential energy hypersurface these chains experience plays a role in governing the diffusion characteristics. Apparently, the fact that the middle section of C_{12} spans one high-energy region of the zeolite (instead of being completely contained within a single low-energy "valley" as C_6 is) lowers the barrier for diffusion.

The resonant diffusion mechanism is not evident for chains aligned along the zigzag channels. Diffusion along these channels requires that chains conform to the contour of the channel. This means that chains must adopt some *gauche* character at varying positions along the backbone to pass through the zigzag channels. The energy barrier for dihedral angles distorting to accommodate the contour of the zeolite pores is of the same order of magnitude as that imposed by the lattice. Thus, chains diffusing along the zigzag channels are subject to a continuously varying series of potential barriers, which eliminate the conditions under which the resonant diffusion model is valid. In essence, chains diffusing along these more tortuous channels sample a wide distribution of lengths and potential barrier locations. Only chains along the straight channels ([010] direction) satisfy the conditions of the model as being essentially rigid and moving in a static but periodic external potential.

The fact that chains within the resonant diffusion zones have negative activation energies for diffusion deserves some comment. In writing the self-diffusivity as a simple Arrhenius expression in eq 3, it was assumed that diffusion is an activated process. The preexponential factor, D_0, is typically weakly dependent on temperature so that the temperature dependence of D_s comes mainly from the exponential term. The activation energy, E_{act}, is a measure of the free energy barrier height to diffusion and is also assumed to be a constant. For a simple spherical molecule diffusing in the static zeolite lattice, this is an accurate picture. For alkane chains with many internal degrees of freedom, however, this representation is too simplistic. The activation barrier height is a function not only of the static zeolite potential but also of the conformation of the chain within the zeolite. Previous work[36] has shown that alkane conformations within the zeolite channels and the potential of mean force along the channels are strongly dependent on temperature. Additional evidence to support this claim is given below. Thus, the activation energy in eq 3 should actually be temperature dependent (not a constant). The results here indicate that, for chains within the resonant diffusion region, the activation energy for diffusion *increases* with increasing temperature. This causes the self-diffusivity to decrease with increasing temperature and the apparent activation energy (given by eq 3) to be negative. Note that the actual activation energy (i.e. the free energy barrier for diffusion) is not negative, simply the apparent activation energy given by eq 3.

The temperature dependence of the activation energy can be explained physically in the following way. Increasing temperature has the effect of broadening the chain length distribution and thus reducing the number of occasions for which a chain is at the resonance length (see Figure 6). Chains can be thought of as becoming more "flexible" as temperature is increased. With this increased flexibility, a chain does not remain in the optimal resonance conformation but rather moves rapidly between different conformations. Since the resonance conformation has the lowest barrier to diffusion, chains that remain in a resonance conformation should experience a lower diffusion barrier (over time) and thus have a higher self-diffusivity. In essence, increased thermal energy "turns off" the resonance effect by allowing chains to quickly thermalize in a low-energy state,

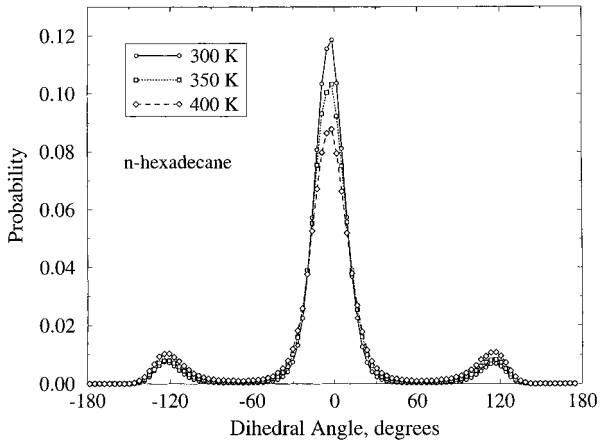

Figure 8. Dihedral angle distribution for *n*-C_{16} at various temperatures. A dihedral angle of 0° corresponds to a *trans* conformation, and ±120° correspond to *gauche* conformations.

while at low temperature the chains behave more like the rigid rods around which the theory was developed. Evidence for this behavior can be seen by examining Figure 8, which shows the effect temperature has on dihedral angle distributions for *n*-C_{16}. Other chain lengths show similar trends. A large fraction of the dihedral angles are centered at the *trans* (0°) position, with only a small fraction of the angles at the two *gauche* (+/− 120°) positions. This distribution is very different from the behavior seen in bulk fluids, where a larger percentage of dihedral angles are in the *gauche* position. The confining nature of the zeolite pores forces the chains to extend and severely limits chain flexibility. If the dihedral angle distributions are computed as a function of chain shape, the distribution becomes even more sharply peaked about the *trans* location for chains located in the straight channels. However, increasing the temperature reduces the fraction of dihedral angles in the *trans* position and increases the fraction of *gauche* angles. This is a measure of the increasing chain flexibility that comes with increasing temperature. Thus it is expected that the resonant diffusion effect will be reduced at higher temperature, which is actually observed in Figure 4. If the interpretation here is correct, then the resonant diffusion effect would be even more pronounced at temperatures below 300 K where the thermal energy is much lower than the activation barrier for dihedral angle motion. Future simulation studies could be carried out to test this hypothesis.

While the relative maxima in $D_{s,yy}$ for C_8 and C_{16} can be explained with the resonant diffusion model, it is not immediately clear why $D_{s,yy}$ is actually *higher* for C_{16} than for C_8. We believe this is due to two factors. First, by examining the chain length distributions in Figure 6 in greater detail, we found that *n*-C_{16} actually matches the lattice periodicity slightly better than does *n*-C_8. A second factor that helps account for the enhanced values of $D_{s,yy}$ for *n*-C_{16} relative to *n*-C_8 is that long chains in silicalite are actually more "rigid" than short chains. This is somewhat counterintuitive, since longer chains can generally adopt more conformations in the bulk phase and so would appear to be more flexible. However, dihedral angle distributions and rotational characteristics indicate that chain rigidity increases with increasing chain length inside the zeolite. We discuss dihedral angle distributions first. By integrating the peaks in plots such as the one in Figure 8 for each chain length and temperature, an estimate of the fraction of dihedral angles in the *trans* and *gauche* states was obtained. Figure 9 shows the result of this calculation. The percentage of dihedral angles in the *trans* position increases as chain length increases. While 80% of the C_8 dihedral angles can be associated with

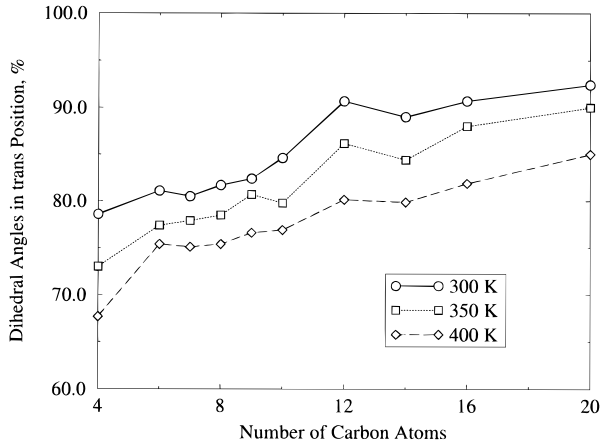

Figure 9. Fraction of dihedral angles in the *trans* position as a function of temperature and chain length.

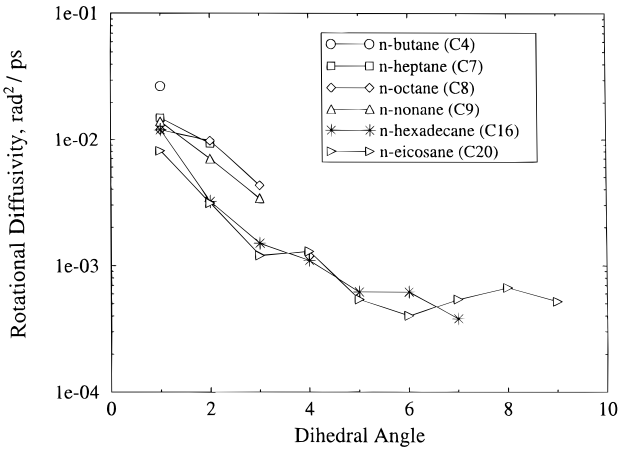

Figure 10. Rotational diffusion coefficients for dihedral angles at 300 K. Dihedral angles are numbered such that 1 corresponds to an end angle, with increasing values corresponding to dihedral angles closer to the chain midpoint. Since the chains are symmetric, equivalent dihedral angles were averaged over.

the *trans* position at 300 K, nearly 90% of the C_{16} angles are in this position. If *gauche* defects can be considered a measure of the flexibility of the chain backbone, then these data indicate that increasing the chain length leads to increased backbone rigidity. The longer chains can thus be expected to be better candidates for resonant diffusion. Note that the dihedral angle distributions will depend on the type of zeolite as well as chain length. Recent calculations by Bates et al.[68] suggest that the fraction of dihedral angles in the *trans* position also increases as a function of chain length for *n*-alkanes in small pore zeolites such as mordenite and ferrierite, but not in more open zeolites such as faujasite. Bandyopadhyay and Yashonath[19] have reported that *gauche* conformations are actually favored over *trans* conformations for *n*-butane in zeolite Y.

As an additional measure of chain rigidity, the rate at which dihedral angles move between *trans* and *gauche* conformations was characterized by computing a "rotational diffusion coefficient" for the dihedral angles as a function of location along the chain backbone. The rotational diffusion coefficient is defined in a manner analogous to eq 1

$$D_\phi = \langle(\phi(t + \Delta t) - \phi(t))^2\rangle/\Delta t \qquad (5)$$

where ϕ is the dihedral angle. Note that unlike the MSD used in eq 1, ϕ is bounded. This means that $\langle(\phi(t + \Delta t) - \phi(t))^2\rangle$ approaches an asymptotic value as $\Delta t \rightarrow \infty$. We avoid this problem by allowing each (*gauche* +) $\rightleftharpoons$ (*gauche* −) transition over time δt to contribute a value of π to the average of $(\phi(t + \delta t) - \phi(t))^2$. The net result is that a plot of the mean square difference in the dihedral angles as a function of time yields a linear relationship, the slope of which gives D_ϕ. We assume that D_ϕ is a good measure of the rate at which rotation about a dihedral angle occurs. That is, a higher D_ϕ implies a more rapid rotation about that particular dihedral angle.

Figure 10 shows the computed rotational diffusivities as a function of chain length and dihedral angle location at 300 K.

Dihedral angle 1 is defined as the angle closest to the end of the chain, angle 2 is the second angle from the end of the chain, etc. The highest numbers correspond to angles near the middle of the chain. Since the chains and dihedral potentials are symmetric, results for equivalent angles were averaged together. This explains why *n*-heptane is listed as having only two dihedral angles. Figure 10 shows that, for all chain lengths, rotation about the dihedral angles near the ends of a chain is faster than rotation about angles near the middle of a chain. Furthermore, rotation about dihedral angles near the middle of chains becomes slower as chain length increases; for *n*-C_{16} and *n*-C_{20}, D_ϕ plateaus for angles 5 and higher at a value near 1×10^{-3} rad/ps. Rotation about these bonds is extremely sluggish. The most facile rotations take place about the single butane dihedral angle. For all chains longer than butane, the value of D_ϕ for the dihedral angle closest to the end of the chain is nearly independent of chain length. This type of behavior can be understood in the following way. Suppose a single dihedral angle near the middle of a chain is changed from a *trans* state to a *gauche* state. For a short chain such as *n*-butane, the resulting change in position of the end atoms will be relatively small. However, as the chain length increases, the relative change in end atom positions as a result of a small change in a middle section dihedral angle gets very large. Large displacements of end atoms are prohibited in the confining pores of the zeolite, and so these types of *trans* → *gauche* rotations are slow and difficult for long chains. Rotation about central dihedral angles of long chains must occur through a cooperative "concerted" motion, involving multiple dihedral angle distortions. Such moves are hindered in the confining regions of the zeolite, which explains the trends seen in Figure 10. (The difficulty with which dihedral angles can be rotated in the middle of long chains is well-known to those who have conducted Monte Carlo simulations of dense polymeric systems. Simple "crankshaft" moves of dihedral angles fail, and elegant methods must be used to more effectively probe the configuration space for polymers[69]). It is clear from Figure 10 that rotation about the dihedral angles in *n*-C_8 is more facile than in *n*-C_{16}. This fact, along with increasing tendency for long chains to adopt *trans* conformations, supports the conclusion that within the zeolite pores the long chain is "stiffer" than the short chain. We believe that, along with differences in the resonance parameter, λ, this increased rigidity accounts for the enhancement of $D_{s,yy}$ for *n*-C_{16} relative to *n*-C_8.

By visualizing the trajectories of the chains, additional insight into the diffusion process was gained. Similar to what Hernández and Catlow[26] have reported for *n*-C_4 and *n*-C_6 in silicalite, chains appear to move by a "hopping" mechanism. Over relatively long periods of time, chains remain localized in low-energy states. Motion during these times consists of "shuttling" back and forth within the zeolite channel over distances of a few angstroms, combined with subtle dihedral angle distortions. Infrequently, the chains become perfectly oriented with the channel contour and execute a hop to another low-energy state. Along the zigzag channels, these hops typically take place over a distance of roughly 5 Å. Changes in channel contour require chains to adopt new conformations

before moving further through the channels. On the other hand, hops along the straight channels occur over much longer distances. Once a chain is aligned along the straight channel, it "sees" an essentially constant channel contour. Hops along the straight channels typically cover 10 Å as the chain moves over a single potential barrier. Interestingly, the chains that are at the resonance lengths (C_8 and C_{16}) often jump over two potential barriers, covering roughly 20 Å in one hop "event". Once a chain of resonance length begins a hop event, it feels little resistance to motion from the zeolite but "skips" over the potential energy barriers. As thermal fluctuations cause intramolecular reorientation, the chain loses its resonance conformation and thermalizes in a low-energy state. This is the same physical picture that was used in developing the resonant diffusion models. It also explains why the resonance effect is diminished at higher temperatures; the intramolecular reorientation rates that kill the resonance effect are greater at high temperature.

A more quantitative description of the hopping mechanism can be obtained in the following way. Let us consider a hopping event as occurring over some short time t_e. An average "jump length" in direction α, J_α, can be defined by tracking the net displacement of a chain center of mass over t_e and averaging this over all chains. That is

$$J_\alpha \equiv \langle |r_\alpha(t_e) - r_\alpha(0)| \rangle \qquad (6)$$

where r_α refers to the α-component of the chain center of mass and the pointed brackets designate an ensemble average. J_x corresponds to jumps along the zigzag channels and J_y to jumps along the straight channels. J_z corresponds to displacements in the *Z*-direction, which has no defined pore system. Table 3 lists the values for J_α at each temperature and for each chain length, where the time for a hopping event was $t_e = 10$ ps. As expected, the average jump distance along the straight channels is larger than that along the zigzag channels, reflecting the enhanced mobility of the chains along the straight channels. We see that J_x decreases steadily as chain length increases and as temperature decreases, reflecting the difficulty with which long chains move along the tortuous zigzag channels. The difference between J_y and J_x is largest for C_8 and C_{16}, again reflecting the resonant diffusion mechanism for these chains. In addition we see that, for nonresonance chain lengths, J_y increases with increasing temperature. For C_8, however, J_y is essentially independent of temperature, while for C_{16} J_y actually decreases with increasing temperature. This is consistent with the observation that chains at the resonance lengths have a negative apparent activation energy for diffusion. J_z is on the order of 1 Å for the shortest chains, indicative of a "rattling" motion within the 5.5 Å diameter pores. J_z decreases to about 0.5 Å for the longest chains, which reflects the fact that center of mass motion normal to the pore axes becomes diminished as chains span an intersection region.

A better understanding of the mechanism of diffusion can be obtained by examining the *distribution* of jump lengths. Most jump events over t_e result in very small displacements of the chain center of mass. What is most interesting from the standpoint of diffusion, however, is the small fraction of jumps that result in large displacements of the chain. Figure 11 shows that portion of the jump distribution plots for *n*-C_6 and *n*-C_{16} at 300 K in which jumps longer than 1 Å take place. It can be seen that the shorter C_6 chains exhibit finite probabilities of jumping between potential barriers (separated by ca. 10 Å) along both the straight and zigzag channels. A small fraction of the chains jump over more than one barrier along the straight channels. For the longer C_{16} chains, no jumps greater than ca. 3 Å occur along the zigzag channels. However, a significant fraction of the jump events along the straight channels are over distances greater than the 10 Å distance between barrier heights.

TABLE 3: Average Displacement in Å of Chain Center of Mass over 10 ps[a]

N	*q*	*T*	J_x	J_y	J_z
4	0	300	1.74	2.41	1.00
6	0	300	1.42	2.22	0.82
7	0	300	1.21	2.48	0.79
8	0	300	1.04	2.95	0.77
9	0	300	0.89	2.83	0.70
10	0	300	0.74	2.62	0.65
12	0	300	0.54	2.68	0.54
14	0	300	0.51	2.62	0.49
16	0	300	0.48	3.80	0.46
20	0	300	0.44	2.53	0.43
6	0.5	300	1.32	2.06	0.76
7	0.5	300	1.17	2.32	0.77
8	0.5	300	0.83	2.88	0.53
9	0.5	300	0.67	2.71	0.46
10	0.5	300	0.76	2.19	0.64
6	5.3	300	0.76	1.48	0.56
8	4.0	300	0.88	1.02	0.69
12	2.7	300	0.68	0.82	0.55
16	2.0	300	0.50	1.26	0.45
4	0	350	2.10	2.97	1.24
6	0	350	1.69	2.51	0.99
7	0	350	1.45	2.62	0.95
8	0	350	1.27	2.93	0.91
9	0	350	1.12	2.85	0.85
10	0	350	0.98	2.55	0.80
12	0	350	0.74	2.73	0.67
14	0	350	0.65	2.53	0.60
16	0	350	0.54	3.48	0.53
20	0	350	0.50	2.85	0.47
4	0	400	2.45	3.62	1.49
6	0	400	1.88	2.81	1.23
7	0	400	1.64	2.82	1.08
8	0	400	1.43	3.00	1.01
9	0	400	1.33	2.91	0.98
10	0	400	1.17	2.67	0.93
12	0	400	0.95	2.71	0.80
14	0	400	0.76	2.65	0.71
16	0	400	0.70	2.85	0.65
20	0	400	0.59	2.72	0.55
6	0.5	400	1.82	2.68	1.11
7	0.5	400	1.61	2.60	1.06
8	0.5	400	1.33	2.88	0.91
9	0.5	400	1.27	2.76	0.97
10	0.5	400	1.17	2.40	0.91

[a] *N* is the number of carbon atoms in a chain, and *q* is the loading in molecules/unit cell.

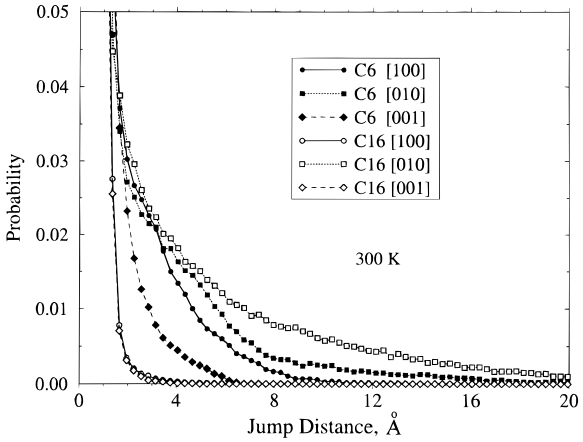

Figure 11. Distribution of jump lengths along the three principle axes over a 10 ps event time for *n*-C_6 and *n*-C_{16} at 300 K.

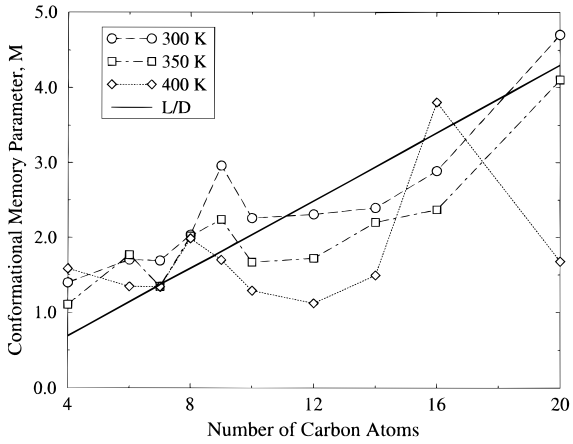

Figure 12. Conformational memory parameter, *M*, versus chain length and temperature. A value of $M = 1$ corresponds to a stochastic diffusion process, while $M > 1$ means that interchange between channels is not favored.

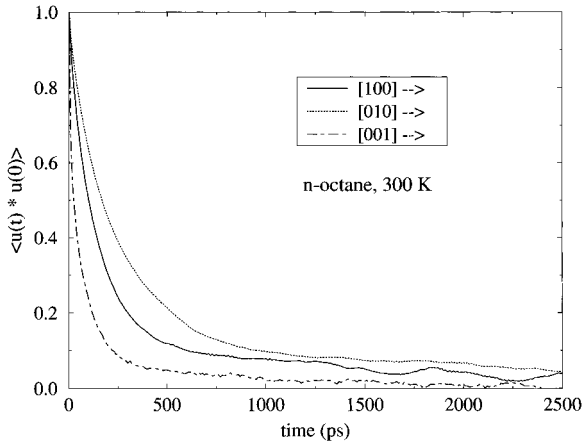

Figure 13. The decay of the three components of $P_1(t)$ versus time for *n*-C_8 at 300 K.

In fact, the probability of C_{16} jumping over multiple barriers is greater than the corresponding probability for C_6. This again indicates that C_{16} chains experience resonant diffusion along the straight channels while C_6 chains do not.

The anisotropy of the self-diffusion tensor was briefly mentioned above. This anisotropy is of practical and theoretical interest.[70] Kärger[71] has proposed the following correlation between the principal values of the diffusivity tensor in silicalite

$$\frac{c^2}{D_{s,zz}} = \frac{a^2}{D_{s,xx}} + \frac{b^2}{D_{s,yy}} \tag{7}$$

where *a*, *b*, *c* are the unit cell edge lengths (20.07, 19.92, and 13.42 Å, respectively). Equation 7 was derived by assuming a stochastic jump process. It should hold for sorbates that quickly lose configurational memory while diffusing. Intuitively, we expect this relation to break down for long chains due to chain connectivity constraints. The conformational memory can be quantified by rearranging eq 7 and defining the parameter *M*:

$$M = \left[\frac{c^2}{D_{s,zz}} \Big/ \left(\frac{a^2}{D_{s,xx}} + \frac{b^2}{D_{s,yy}}\right)\right] \tag{8}$$

For $M = 1$, chains quickly lose conformational memory and readily diffuse between the zigzag and straight channels. For $M > 1$, the diffusivity in the *Z*-direction is suppressed relative to the other directions, indicating slower interchange between the channels. (Recall that motion in the *Z*-direction of silicalite can *only* take place through motion along both the straight and zigzag channels.) Figure 12 is a plot of *M* versus chain length at 300−400 K and infinite dilution. For the very shortest chains, *M* is indeed close to 1, which means the short chains can easily interchange between the two different channel systems. Longer chains tend to become localized within a given channel system, and this tendency increases as chain length increases and temperature decreases. It is reasonable to expect that this localization phenomenon is primarily due to geometric constraints. To test this, the ratio of the most probable chain length at 300 K to the average pore diameter, *L*/*D*, was computed and plotted as the solid line in Figure 12. This ratio should reflect the ease with which a rigid chain can "turn the corner" in moving from one channel system to another. It can be seen that *L*/*D* captures the basic trend in Figure 12 for low temperatures. At higher temperatures, the trend is not so clear. Nonresonance chains (C_{12}, C_{20}) have reduced conformational memories at 400 K. Apparently these chains are of just the right length to make channel interchange more facile at high temperature.

As another means of quantifying the interchange rate between channel systems, one can look at the decorrelation of the normalized end-to-end vector, $\boldsymbol{u}(t)$, which describes the orientation of the alkane in the zeolite pore.[24] The decorrelation of this vector as a function of time can be studied through the first Legendre polynomial, $P_1(t)$:

$$P_1(t) = \langle \mathbf{u}(t)\cdot\mathbf{u}(0)\rangle = \langle u_x(t)\cdot u_x(0)\rangle + \langle u_y(t)\cdot u_y(0)\rangle + \langle u_z(t)\cdot u_z(0)\rangle \tag{9}$$

Since the channels of silicalite are orthogonal, the rate at which $P_1(t)$ decays gives an indication of the interchange rate between different channel systems. Assuming that $P_1(t)$ decays to zero at long times, a time constant for this interchange, τ, can be estimated from the following equation

$$\tau = \int_0^\infty P_1(t)\, \mathrm{d}t \tag{10}$$

There are two difficulties with the use of eq 10. First, since the occupancy of the straight channels is somewhat greater than the zigzag channels for the longest chains, $P_1(t)$ will not necessarily decay to zero for these chains. Second, even if $P_1(t)$ went to zero, the decay time for the longest chains is much longer than what can be tracked with MD. This prevents the accurate determination of τ for long chains. Nevertheless, an estimate of the interchange time constant can be obtained by assuming that beyond the longest simulation time, t_0, $P_1(t)$ decays exponentially. Using this approximation, τ becomes

$$\tau = \int_0^\infty P_1(t)\, \mathrm{d}t \approx \frac{\int_0^{t_0} P_1(t)\, \mathrm{d}t}{1 - P_1(t_0)} \tag{11}$$

Figure 13 shows a typical plot of the decay of $P_1(t)$ as a function of time for *n*-C_8 at 300 K. Notice that chains leave the straight channels ([010] direction) at the slowest rate. The decorrelation of the end-to-end vector along the [001] direction, which does not have a channel system, is relatively fast and is due to the "rocking" motion of the chains within a channel.[24] Using eqs 10 and 11, estimates of the time constant for channel interchange can be obtained from data such as that shown in Figure 13. Figure 14 shows the results for τ as a function of chain length at 300 K, while Table 4 provides a complete listing of all computed time constants. In Figure 14a, it can be seen that the estimated time constant associated with motion out of

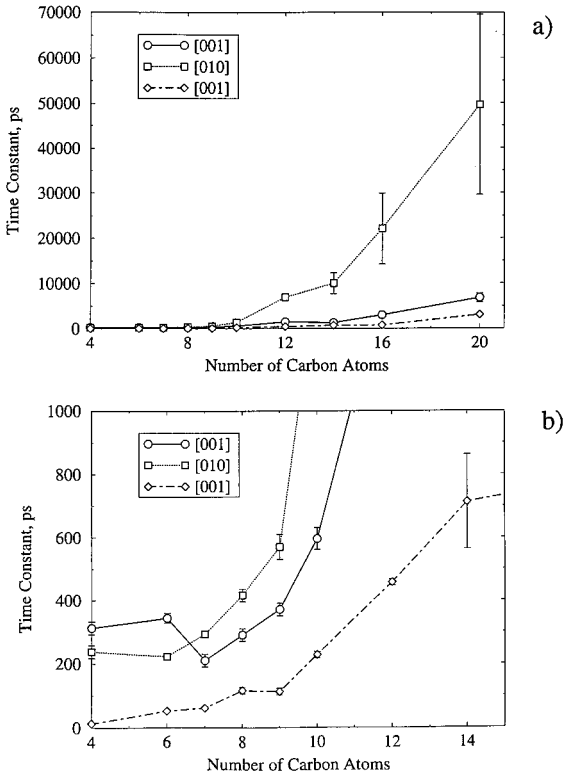

Figure 14. (a) Time constants associated with the interchange between channel sections as a function of chain length at 300 K. (b) Expanded view showing that chains become "frozen" in their respective channels at lengths greater than about *n*-C_8.

the straight channels approaches microsecond time scales for the longest chains. The error bars associated with τ for the longest chains become quite large, as extrapolation to times beyond the actual simulation time becomes necessary. Nevertheless, the general behavior of this system is clear. The longest chains become "frozen" in a given channel system, with the tendency to become frozen in the straight channels being the greatest. In Figure 14b, the scale in Figure 14a is expanded to show that the onset of this localization phenomenon occurs at about C_8-C_9. Chains shorter than this move between the two channel systems with a time constant of ca. 300 ps. However, it is shown below that at finite loadings the interchange time constant for small chains increases dramatically over the infinite dilution results. These data indicate that for long chains and/or high loadings, silicalite becomes essentially a one-dimensional zeolite. (For a true one-dimensional zeolite, single-file diffusion behavior would be expected,[5] which is not seen in this work. Thus, there still is some finite amount of channel interchange.) These results have important implications in catalysis. As pores become blocked with coke or crystal defects, the three-dimensional structure of silicalite enables short chains to circumvent blockages as long as the loading is not too high. Pore blockages have a more drastic effect on intracrystalline diffusivities of long chains, however, since these molecules only slowly move between different channels. This very slow interchange between channel systems may also have implications for the experimental measurement of diffusivities. Macroscopic experiments, such as uptake rate measurements, are inherently nonequilibrium. These techniques measure a time constant for the rate at which a molecule sorbs into the pores of a zeolite. The results of this study indicate that the time constant for interchange *between* different channels can actually be longer than the time constant for diffusion. Thus, a transient experiment may be measuring two simultaneous processes; the first is the diffusion of sorbates into the pores, and the second is the rearrangement of the sorbates *within* the pores. On the other hand, microscopic experiments are performed on systems that are at equilibrium and so only measure the diffusional process (the sorbates have already "rearranged" to their equilibrium positions). If the interchange process is faster than the diffusion process, then the macroscopic experiments should yield diffusivities equal to the microscopic experiments. On the other hand, if the rearrangement time constant is longer than the diffusional time constant, as the present study suggests is the case with long alkanes in silicalite, then the macroscopic measurements will yield "apparent" diffusivities that are smaller than the microscopic experiments. This could provide a partial explanation for the frequent disagreement between these different experimental techniques and why MD tends to agree more with microscopic measurements. Due to the rather large error bars in Figure 14, it is difficult to make a quantitative assessment as to whether such an effect could be responsible for the magnitude of the differences between the methods seen in Figure 3. It must be pointed out, however, that this mechanism cannot explain all the differences between experimentally obtained diffusivities. Large discrepancies are also seen with small molecules, which quickly rearrange inside the zeolite pores. Future simulation studies may help shed more light on this interesting question.

4.2. Finite Loadings. All of the results discussed so far have been for systems where the concentration of sorbates is taken in the infinite dilution limit. We have also carried out simulations to assess the effect finite loading levels have on the equilibrium and dynamic properties of the sorbates. Simulations were conducted at a relatively low loading of 0.5 molecules per unit cell for *n*-C_6 through *n*-C_{10} at 300 and 400 K. A simulation at this loading was also performed for *n*-C_{16} at 300 K. We note that the use of the number of molecules per unit cell as a measure of loading can be misleading when comparing results for different chain lengths. At the same molecular loading, the concentration of methyl and methylene "mers" will be higher for the longer chains. To investigate this further, additional simulations were carried out at 300 K for C_6, C_8, C_{12}, and C_{16} using molecular loadings that correspond to 32 mers per unit cell. Note that this is a fairly high loading for silicalite; there is very little open pore volume at these high concentrations.

In all cases, increasing the loading of a given chain decreased the self-diffusivity. The magnitude with which the self-diffusivity decreases depends on the loading; higher loadings result in significantly lower self-diffusivities. This can be seen most clearly in Figure 15, which shows a plot of D_s at 300 K as a function of chain length and loading. For reference, the infinite dilution results are also shown. Table 1 provides a summary of all the computed diffusivities. In addition to the overall decrease in D_s, we also see that increasing the loading reduces the resonant diffusion effect. At 0.5 molecules per unit cell, the differences between the maxima and minima in D_s are smaller than in the infinite dilution case. At the highest loadings, we see that the resonant diffusion effect is nearly gone; D_s drops at a chain length of C_8 and remains fairly constant after that. This is expected, since the resonant diffusion mechanism relies on the chains hopping over fairly long distances before thermalizing in low-energy states. At high loadings, collisions with neighboring molecules discourage this type of diffusion mechanism. This can also be seen in Figure 16, which shows the distribution of jump lengths along the straight channels over a 10 ps time period for *n*-C_8 and *n*-C_{16}. Average jump lengths at finite loadings are given in Table 3. By comparing the finite loading and infinite dilution results, we see that the fraction of

TABLE 4: Time Constants, τ, in ps for the Decay of $P_1(t)$[a]

		300 K			350 K			400 K		
N	q	τ_x	τ_y	τ_z	τ_x	τ_y	τ_z	τ_x	τ_y	τ_z
4	0	3(1)0	2(4)0	10.(6)	1(6)0	7(9)	6.(1)	9(3)	10(2)	7.(9)
6	0	3(4)0	2(2)0	5(2)	2(1)0	1(9)0	27.(2)	1(6)0	93.(5)	18.(1)
7	0	2(1)0	2(9)0	61.(6)	15(7)	13(6)	36.(1)	88.(3)	12(2)	27.(6)
8	0	2(9)0	4(2)0	11(6)	11(1)	18(2)	50.(4)	10(0)	13(6)	35.(3)
9	0	3(7)0	5(7)0	11(3)	19(1)	30(1)	64.(1)	95.(6)	14(0)	40.(7)
10	0	5(9)0	14(2)0	22(7)	25(9)	47(6)	93.(6)	11(3)	26(9)	60.(1)
12	0	14(9)0	6(9)00	45(7)	50(2)	12(1)0	16(6)	25(2)	56(5)	82.(0)
14	0	13(3)0	1(1)000	5(2)0	8(9)0	18(5)0	22(7)	36(6)	1(4)00	12(0)
16	0	3(0)00	2(2)000	7(1)0	5(2)0	5(7)00	24(2)	38(7)	1(5)00	14(3)
20	0	6(8)00	(7)0000	3(3)00	1(5)00	3(5)000	40(2)	7(3)0	3(8)00	28(0)
6	0.5	3(3)0	2(2)0	3(8)				8(3)	8(5)	18.(9)
7	0.5	20(1)	3(2)0	6(5)				6(6)	9(6)	2(6)
8	0.5	21(3)	32(4)	9(7)				7(1)	10(2)	34.(3)
9	0.5	34(9)	57(9)	10(9)				9(8)	15(2)	4(5)
10	0.5	56(0)	12(5)0	15(7)				15(8)	23(0)	58.(6)
6	5.3	11(8)0	9(7)0	5(8)						
8	4.0	4(3)0	4(5)0	16(1)						
12	2.7	1(3)000	1(5)000	2(9)00						
16	2.0	1(5)000	1(8)000	1(8)00						

[a] The parentheses indicate where the uncertainty in the estimate of τ lies.

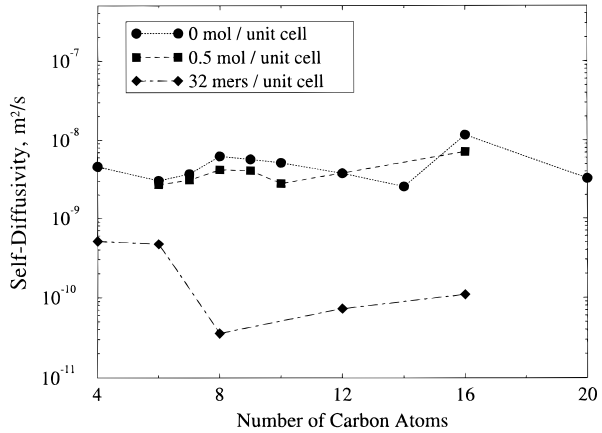

Figure 15. Self-diffusivity at 300 K as a function of chain length and loading. Self-diffusivities at finite loadings are lower than those at infinite dilution. Resonant diffusion effects are damped by the presence of other molecules. The result for n-C_4 at 32 mers per unit cell is taken from ref 24.

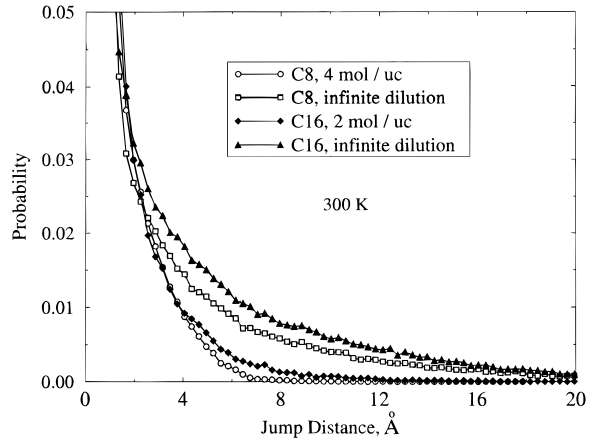

Figure 16. Distribution of jump lengths along the straight channels for n-C_8 and n-C_{16} at 300 K. The fraction of jumps occurring over long distances is reduced at finite loadings due to interactions with neighboring molecules.

jumps occurring over long length scales is much greater for the infinite dilution chains than for the chains at high loadings. Interestingly, for n-C_{16} there are still a significant number of chains that jump distances on the order of 20 Å, even at the higher loadings. This accounts for the fact that the diffusivity of n-C_{16} is still relatively large at high loadings. Apparently, the resonant diffusion mechanism is severely depressed as loading increases, but the effect is still operative to some extent for n-C_{16}, which has the lowest molecular concentration at 32 mers per unit cell.

Static properties such as dihedral angle distributions and chain length distributions were virtually unchanged from the infinite dilution values. The largest change in equilibrium properties occurred when computing the sorbate siting. As has been reported in earlier work,[36] there is a strong tendency for longer chains to segregate in the straight channels of silicalite at low loadings. This tendency grows stronger as chain length increases and temperature decreases. The same thing was observed in our equilibrium MD simulations. At the highest loading levels, chains were forced to populate the zigzag channels at nearly the same levels as the straight channels.

As mentioned above, the time constants for molecular rearrangement were also computed for the finite loading cases using eq 11. These values are given in Table 4. The time constants are nearly the same for the infinite dilution case and for a loading of 0.5 molecules per unit cell. At the highest loadings, however, we see that the time constants increase over the infinite dilution case. The increase is most pronounced for the short chains, which readily exchange between channel systems at low loadings. The effect on longer chains, which already exhibit sluggish interchange rates, is much smaller. These results make sense if one considers that, at the highest loadings, neighboring chains block the paths that a molecule must take to interchange between channels. The probability of two molecules moving simultaneously to enable an interchange is low, which results in the long times seen in Table 4. Interestingly, n-C_8 moves out of the X and Y-channels faster than n-C_6 at the highest loadings. Apparently, n-C_8 is just long enough to allow one end of the chain to "wait" near a channel intersection for a neighboring molecule to move out of its path, while for n-C_6 to interchange it must move into position at the same time as a neighbor moves out of its way.

5. Summary

The results of molecular dynamics simulations for a series of n-alkanes in the zeolite silicalite have been reported. The

computed self-diffusivities and apparent activation energies for diffusion of short chains agree well with "microscopic" measurement techniques such as NMR and neutron scattering. As is the case with many zeolitic systems, transient ("macroscopic") experimental techniques give self-diffusivities that are one or more orders of magnitude smaller than the simulations and microscopic methods. To our knowledge, only one set of macroscopic measurements have been made that investigate the diffusivity of chains longer than *n*-hexane in silicalite. Not surprisingly, the simulations predict higher values of the diffusivity than what the macroscopic measurements yield. It is interesting to note, however, that the self-diffusivity plateaus at a nearly constant value for chains longer than *n*-octane in both the simulations and the macroscopic experiment. This behavior is contrary to what is seen in a homogeneous phase where the self-diffusivity is a steadily decreasing function of chain length. Upon investigation of the individual components of the self-diffusivity tensor, an explanation for this unusual behavior was proposed on the basis of a resonant diffusion mechanism for certain chain lengths along the straight channels of silicalite.

Resonant diffusion effects for alkane/zeolite systems were predicted theoretically several years ago. The present study confirms the essential elements of the theories. An enhancement of the self-diffusivities and reduction in the apparent activation energies for diffusion were seen for *n*-octane and *n*-hexadecane along the straight channels of silicalite. The effect was not seen along the tortuous zigzag channels. Increasing the temperature damped the resonance effect, as did increasing the sorbate loading. To our knowledge, this is the first molecular simulation study that has witnessed this behavior. The results indicate that additional experimental and simulation work are called for in which the anisotropy of the self-diffusivity tensor in silicalite is examined for chains longer than *n*-hexane. Other zeolite/sorbate systems should also be probed to see if evidence for resonant diffusion effects are present.

Through visualizing trajectories and recording the center of mass displacements of chains as a function of time intervals, it was determined that chains diffuse via a "jumping" mechanism. Much of the time, chains reside within low-energy conformations, executing subtle librations and rocking motions. Infrequently, a chain will become positioned in such a way so as to execute a long (ca. 5−10 Å) "hop" before thermalizing in another potential minima. The rate of thermalization is enhanced by increases in temperature and channel tortuosity. Thus, chains hop farther along the straight channels than the zigzag channels, which accounts for the anisotropy in the self-diffusivity tensor. Chains at the resonance lengths have an even more difficult time thermalizing. They "skip" across across multiple potential energy barriers before thermalizing, which accounts for their enhanced diffusion coefficients. Interestingly, longer chains appear to have more rigid backbones in the pores than short chains, which leads to a greater resonance effect for these chains.

The rates at which chains move from one channel system to another were also estimated by computing the time it takes for the chain end-to-end vector to become decorrelated. It was found that the interchange time for chains as short as *n*-octane is rather small, on the order of hundreds of picoseconds. This interchange time increases dramatically as loading increases but decreases as temperature increases. The interchange time for the longest chains is high (approaching microseconds), regardless of loading. For some chains, the channel interchange time constant is longer than the time constant for diffusion. The rate at which chains leave the straight channels is considerably smaller than the rate at which chains leave the zigzag channels. The implication is that silicalite is a three-dimensional zeolite for short chains but effectively becomes a one-dimensional zeolite for the longest chains. This is important when considering the effects of pore blocking and coking on the transport of chains in silicalite. It may also help explain part of the reason why transient experiments can yield diffusivities that are smaller than the inherent equilibrium microscopic methods. If rearrangement of sorbates *within* the pores of a zeolite takes longer than diffusion, then a transient experiment will extract a time constant that is a convolution of these two processes. An equilibrium method, on the other hand, will only record the diffusional process. Unfortunately, obtaining precise rearrangement time constants is difficult for the long chains, so we cannot quantify how important this effect is.

Increasing the sorbate loading has the effect of decreasing the computed self-diffusivity for all chain lengths. The resonant diffusion mechanism along the straight channels is suppressed, because long distance hopping motions are frustrated by the presence of neighboring molecules. At finite loadings, equilibrium properties such as torsion angle distributions were only slightly different than those obtained in the infinite dilution limit. This confirms that the zeolite−sorbate interactions dominate the conformational properties of the sorbate for this system.

The simulations presented here suggest that resonant diffusion is a real effect in zeolites but that it will only occur under highly specialized conditions. Low temperature, rigid sorbates, smooth channels, and low loadings are all required for the mechanism to be operative. These conditions will rarely be met under practical conditions. Moreover, the effect is fairly small for alkanes in silicalite; enhancements in D_s by a factor of 2 or so were observed. All of this could help explain why resonant diffusion effects are difficult to observe experimentally. While these simulations have not been carried out on the same system as that used by Gorring,[43] they do suggest that the *dramatic* (i.e. orders of magnitude) enhancements in the self-diffusivity at certain chain lengths reported in that work may be due to other effects. Additional experimental and computational work needs to be done to confirm this, however. A recently developed technique in which PFG NMR is used with oriented zeolite crystals[72] may be particularly useful in this regard.

Acknowledgment. E.J.M. thanks Prof. R. Q. Snurr for several helpful discussions. Profs. A. T. Bell and D. N. Theodorou are thanked for encouragement in initiating this work.

References and Notes

(1) Satterfield, C. N. *Heterogeneous Catalysis in Practice*; McGraw-Hill: New York, 1980.

(2) Yang, R. T. *Gas Separation in Adsorption Processes*; Butterworth Publishers: Stoneham, MA, 1987.

(3) Bein, T. *Chem. Mater.* **1996**, *8*, 1636−1653.

(4) Weisz, P. B. *CHEMTECH* **1973**, *3*, 498−505.

(5) Kärger, J.; Ruthven, D. M. *Diffusion in Zeolites and Other Microporous Solids*; Wiley-Interscience: New York, 1992.

(6) Hufton, J. R.; Ruthven, D. M. *Ind. Eng. Chem. Res.* **1993**, *32*, 2379−2386.

(7) Van-Den-Begin, N.; Rees, L. V. C.; Caro, J.; Bülow, M. *Zeolites* **1989**, *9*, 287−292.

(8) The Wicke−Kallenbach method as applied to zeolites was pioneered by Paravar and Hayhurst[9] and Wernick and Osterhuber.[10] Refinements to the technique have been reported by Sun el al.[11]

(9) Paravar, A. R.; Hayhurst, D. T. *Proceedings of the 6th International Zeolites Conference*; Olson, D., Bisio, A., Eds.; Butterworths: Buildford, England, 1984.

(10) Wernick, D. L.; Osterhuber, E. J. *J. Membr. Sci.* **1985**, *22*, 137−146.

(11) Sun, M. S.; Talu, O.; Shah, D. B. *AIChE J.* **1996**, *42*, 3001−3007.

(12) Heink, W.; Kärger, J.; Pfeifer, H.; Stallmach, F. *J. Am. Chem. Soc.* **1990**, *112*, 2175−2178.

(13) Jobic, H.; Beé, M.; Kearley, G. J. *J. Phys. Chem.* **1994**, *98*, 4660−4665.
(14) Allen, M. P.; Tildesley, D. J. *Computer Simulation of Liquids*; Clarendon Press: Oxford, U.K., 1987.
(15) Frenkel, D.; Smit, B. *Understanding Molecular Simulation*; Academic Press: San Diego, CA, 1996.
(16) Bell, A. T.; Maginn, E. J.; Theodorou, D. N. Molecular Simulation of Adsorption and Diffusion in Zeolites. In *Handbook of Heterogeneous Catalysis*; Ertl, G., Knözinger, H., Weitkamp, J., Eds.; VCH: Weinheim, in press.
(17) Panagiotopoulos, A. Z. *Fluid Phase Equilib.* **1996**, *116*, 257−266.
(18) Haile, J. M. *Molecular Dynamics Simulation: Elementary Methods*; Wiley: New York, 1992.
(19) Bandyopadhyay, S.; Yashonath, S. *J. Chem. Phys.* **1996**, *105*, 7223−7226.
(20) Klein, H.; Fuess, H.; Schrimpf, G. *J. Phys. Chem.* **1996**, *100*, 11101−11112.
(21) Demontis, P.; Yashonath, S.; Klein, M. L. *J. Phys. Chem.* **1989**, *93*, 5016−5019.
(22) Schrimpf, G.; Tavitian, B.; Espinat, D. *J. Phys. Chem.* **1995**, *99*, 10932−10941.
(23) Snurr, R. Q.; Bell, A. T.; Theodorou, D. N. *J. Phys. Chem.* **1994**, *98*, 11948−11961.
(24) June, R. L.; Bell, A. T.; Theodorou, D. N. *J. Phys. Chem.* **1992**, *96*, 1051.
(25) Goodbody, S. J.; Watanabe, K.; MacGowan, D.; Walton, J. P. R. B.; Quirke, N. *J. Chem. Soc., Faraday Trans.* **1991**, *87*, 1951−1958.
(26) Hernández, E.; Catlow, C. R. A. *Proc. R. Soc. London A* **1995**, *448*, 143−160.
(27) Titiloye, J. O.; Parker, S. C.; Stone, F. S.; Catlow, C. R. A. *J. Phys. Chem.* **1991**, *95*, 4038−4044.
(28) Catlow, C. R. A.; Freeman, C. M.; Vessal, B.; Tomlinson, S. M.; Leslie, M. *J. Chem. Soc., Faraday Trans.* **1991**, *87*, 1947−1950.
(29) Smit, B.; Siepmann, J. I. *Science* **1994**, *264*, 1118−1120.
(30) Smit, B.; Siepmann, J. I. *J. Phys. Chem.* **1994**, *98*, 8442−8452.
(31) Van Well, W. J. M.; Wolthuizen, J. P.; Smit, B.; Van Hoof, J. H. C.; et al. *Angew. Chem. Int. Ed. Engl.* **1995**, *34*, 2543−2544.
(32) Smit, B.; Maesen, T. L. N. *Nature* **1995**, *374*, 42.
(33) Smit, B. *J. Phys. Chem.* **1995**, *99*, 5597−5603.
(34) Smit, B. *Mol. Phys.* **1995**, *85*, 153−172.
(35) Maginn, E. J.; Bell, A. T.; Theodorou, D. N. Low-Occupancy Sorption Thermodynamics of Long Alkanes in Silicalite Via Molecular Simulation. In *Zeolites and Related Microporous Materials: State of the Art 1994*; Weitkamp, J., Karge, H. G., Pfeifer, H., Hölderich, W. F., Eds.; Studies in Surface Science and Catalysis 84; Elsevier Science Publishers B.V.: Amsterdam, 1994.
(36) Maginn, E. J.; Bell, A. T.; Theodorou, D. N. *J. Phys. Chem.* **1995**, *99*, 2057−2079.
(37) Sun, M. S.; Talu, O.; Shah, D. B. *J. Phys. Chem.* **1996**, *100*, 17276−17280.
(38) Eic, M.; Ruthven, D. M. *Zeolites: Facts, Figures, Future*; Jacobs, P. A., van Santen, R. A., Eds.; Studies in Surface Science and Catalysis 49B; Elsevier: Amsterdam, 1989.
(39) Recent work by Fichthorn and co-workers on the development of "smart Monte Carlo" simulation methods could enable the approximate calculation of diffusivities less than 10^{-9} m^2/s. See, for example: Kumar, P. V.; Raut, J. S.; Warakomski, S. J.; Fichthorn, K. A. *J. Chem. Phys.* **1996**, *105*, 686−695.
(40) Caro, J.; Bülow, M.; Schirmer, W.; Kärger, J.; Heink, W.; Pfeifer, H.; Ždanov, S. P. *J. Chem. Soc., Faraday Trans. 1* **1985**, *81*, 2541−2550.
(41) Maginn, E. J.; Bell, A. T.; Theodorou, D. N. *J. Phys. Chem.* **1996**, *100*, 7155−7173.
(42) Heink, W.; Kärger, J.; Pfeifer, H.; Datema, K. P.; Nowak, A. K. *J. Chem. Soc., Faraday Trans.* **1992**, *88*, 3505−3509.
(43) Gorring, R. L. *J. Catal.* **1973**, *31*, 15−26.
(44) Ruckenstein, E.; Lee, P. S. *Phys. Lett.* **1976**, *56A*, 423−424.
(45) Nitsche, J. M.; Wei, J. *AIChE J.* **1991**, *37*, 661−670.
(46) Tsekov, R.; Ruckenstein, E. *J. Chem. Phys.* **1994**, *100*, 3808−3812.
(47) Derouane, E. G.; Andre, J.-M.; Lucas, A. A. *J. Catal.* **1988**, *110*, 58−73.
(48) Yashonath, S.; Santikary, P. *J. Chem. Phys.* **1994**, *100*, 4013−4016.
(49) Zeolite T is an intergrowth of erionite and offretite, made up primarily of offretite. See: Szostal, R. *Handbook of Molecular Sieves*; Van Nostrand Reinhold: New York, 1992.
(50) The orthorhombic silicalite structure has been shown to undergo a reversible phase transition at about 330 K to a structure having monoclinic symmetry. Below this temperature, the monoclinic form is most stable, and above it, the orthorhombic form is most stable (Hay, D. G.; Jaeger, H.; West, G. W. *J. Phys. Chem.* **1985**, *89*, 1070−1072). However, it is also known that the adsorption of small molecules can stabilize the orthorhombic form, even at temperatures below the transition temperature (Kokotailo, G. T.; Fyfe, C. A.; Kennedy, G. J.; Gobbi, G. C.; Strobl, H.; Pasztor, C. T.; Barlow, G. E.; Bradley, S.; Murphy, W. J.; Ozubko, R. S. *Pure Appl. Chem* **1986**, *58*, 1367−1374). For this reason, we believe we are justified in using the orthorhombic form throughout this work.
(51) Olson, D. H.; Kokotailo, G. T.; Lawton, S. L.; Meir, W. M. *J. Phys. Chem.* **1981**, *85*, 2238−2243.
(52) Demontis, P.; Fois, E. S.; Suffritti, G. B.; Quartieri, S. *J. Phys. Chem.* **1990**, *94*, 4329−4334.
(53) June, R. L.; Bell, A. T.; Theodorou, D. N. *J. Phys. Chem.* **1991**, *95*, 8866−8878.
(54) Edberg, R.; Evans, D. J.; Morriss, G. P. *J. Chem. Phys.* **1986**, *84*, 6933−6939.
(55) The potential parameters for bond angle fluctuations were taken from van der Ploeg et al. (van der Ploeg, P.; Berendson, H. J. C. *J. Chem. Phys.* **1982**, *76*, 3271−3276), while the torsion potential was originally given by Ryckaert et al. (Ryckaert, J. P.; Bellemans, A. *Faraday Discuss. Chem. Soc.* **1978**, *66*, 95−106).
(56) See, for example: Jorgensen, W. L.; Madura, J. D; Swenson, C. J. *J. Am. Chem. Soc.* **1984**, *106*, 6638−6646. Rodríguez, A. L.; Vega, C.; Freire, J. J.; Lago, S. *Mol. Phys.* **1991**, *73*, 691−701. Smit, B.; Karaborni, S.; Siepmann, J. I. *J. Chem. Phys.* **1995**, *102*, 2126−2139.
(57) An all-atom model is currently being investigated. This model is similar to the CVFF and PCFF forcefields used in the commercial software package offered by MSI, San Diego, CA.
(58) Gear, C. W. *Numerical Initial Value Problems in Ordinary Differential Equations*; Prentice Hall: Englewood Cliffs, NJ, 1971.
(59) Berendsen, H. J. C.; Postma, J. P. M.; Van Gunsteren, W. F.; Di Nola, A.; Haak, J. R. *J. Chem. Phys.* **1984**, *81*, 3684−3690.
(60) For example, see refs 24−26.
(61) The code used in this work originated from the work of R. L. June.[24] Modifications were made to enable longer chains to be simulated efficiently A typical simulation involving *n*-C_{12} took roughly 3 CPU hours per ns of simulation time on a Sun Ultra 170 workstation.
(62) Besides the requirement that the MSD be linear, the MSD should be greater than the square of the unit cell edge length to ensure that molecules are not trapped in localized regions within the zeolite. In most cases this requirement was met. For the longest chains at the lowest temperatures the MSD in the *X* and *Z*-directions was often less than the square of the unit cell edge length in these directions. In all cases, however, the MSD for motion in the *Y*-direction met the criterion of being at least as great as the square of the unit cell edge length. Because the self-diffusivity is dominated by $D_{s,yy}$, our confidence in the values of D_s and $D_{s,yy}$ is therefore high. The reliability of the values for $D_{s,xx}$ and $D_{s,zz}$ is not as great, but our estimates represent upper bounds on their values. Even taking $D_{s,xx}$ and $D_{s,zz}$ to be zero does not change the qualitative features or the order of magnitude of D_s.
(63) Maginn, E. J.; Bell, A. T.; Theodorou, D. N. *J. Phys. Chem.* **1993**, *97*, 4173−4181.
(64) Smith, G. D.; Yoon, D. Y. *J. Chem. Phys.* **1994**, *100*, 649−658.
(65) Jobic, H.; Beé, M.; Kearley, G. J. *Zeolites* **1989**, *9*, 312−317.
(66) Jobic, H.; Beé, M.; Kearley, G. J. *Zeolites* **1992**, *12*, 146−151.
(67) In essence, the concept of a "negative" activation energy makes no sense in terms of the classic concept of an activated process. Nevertheless, we report values for the apparent activation energy as a means of quantifying the temperature dependence of the self-diffusivity.
(68) Bates, S. P.; van Well, W. J. M.; van Santen, R. A.; Smit, B. *J. Phys. Chem.* **1996**, *100*, 17573−17581.
(69) Dodd, L. R.; Boone, T. D.; Theodorou, D. N. *Mol. Phys.* **1993**, *78*, 961−996.
(70) Faux, D. A.; Hall, C. K.; Sundaresan, S. *Chem. Eng. Sci.* **1991**, *46*, 2359−2362.
(71) Kärger, J. *J. Phys. Chem.* **1991**, *95*, 5558−5560.
(72) Hong, U.; Kärger, J.; Kramer, R.; Pfeifer, H.; Seiffert, G.; Müller, U.; Unger, K. K.; Lück, H. -B.; Ito, T. *Zeolites* **1991**, *11*, 816−821.